Propane Clusters in Titan's Lower Atmosphere: Insights from a Combined Theory/Laboratory Study

Jérémy Bourgalais, Olivier Durif, Sébastien D. Le Picard, P. Lavvas, F Calvo, S Klippenstein, Ludovic Biennier

MNRAS **000**, 1–10 (2019) Preprint 21 June 2019 Compiled using MNRAS LATEX style file v3.0

Propane Clusters in Titan's Lower Atmosphere: Insights from a Combined Theory/Laboratory Study

J. Bourgalais,[1] O. Durif,[1] S. D. Le Picard,[1] P. Lavvas,[2] F. Calvo,[3] S. J. Klippenstein,[4] and L. Biennier[1]⋆

[1] *Institut de Physique de Rennes, UMR 6251 CNRS-Université de Rennes 1, 263 avenue Général Leclerc 35042 Rennes, France.*
[2] *Groupe de Spectrométrie Moléculaire et Atmosphérique UMR CNRS 7331, Université de Reims Champagne-Ardenne, 51687 Reims, France.*
[3] *Univ. Grenoble Alpes, CNRS, LIPhy, 38000 Grenoble, France.*
[4] *Chemical Sciences and Engineering Division, Argonne National Laboratory, Argonne, IL 60439, USA.*

Accepted - - . Received - -; in original form - -

ABSTRACT

In spite of the considerable advances made by Cassini-Huygens in our understanding of Titan, many questions endure. In particular, the detailed processes that lead to the formation of haze aerosols in Titan's atmosphere, found in high concentrations at low altitudes, are not well identified. Hydrocarbons, which are abundant constituents of Titan's cold atmosphere originating from photochemical processes, may simultaneously condense on the surface of existing aerosols, nucleate and grow to generate new aerosol seeds. The relative importance of the various processes depends on several factors, including the saturation ratio. The dynamics of hydrocarbon condensation and nucleation in Titan's atmosphere remains poorly known.

Aiming to progress on these issues, we investigate here the kinetics of propane dimer formation at low temperature through state-of-the-art laboratory experiments combined with theoretical calculations. Our results provide an estimate of the rate coefficients, which are then employed to evaluate the abundance of propane dimers in the lower atmosphere of Titan. The mixing ratios of propane dimers inferred, with a maximum abundance of 10 cm^{-3} near 100 km, is found to be under the detection limit of the Composite Infrared Spectrometer (CIRS) of the Cassini spacecraft.

Based on our results, homogeneous nucleation of the most abundant species appears not to be relevant for the growth of aerosols. Future studies should focus on homogeneous nucleation of polar molecules or alternatively on heterogeneous processes, which are usually more efficient.

Key words: planets and satellites: atmospheres, planets and satellites: individual: Titan, molecular processes

1 INTRODUCTION

A large variety of van der Waals complexes, in which molecules are bound by intermolecular dispersion forces, is expected in planetary atmospheres. The presence of such molecular complexes can affect both chemistry and climate, as the optical properties and reaction dynamics of the constituent monomers are altered by the intermolecular interactions at play (Vaida et al. 2003; Daniel et al. 2004). In particular, dimers as well as any other form of molecular structures whose interaction leads to symmetry breaking of isolated molecules, may cause an excess absorption and therefore play, a significant role in the greenhouse effect (Vigasin & Mokhov 2017). The first extraterrestrial dimer detected was H_2-H_2 in Jupiter's upper atmosphere at 120 K and in Saturn's atmosphere at 85 K, by Frommhold et al. (1984). In addition to their own role on radiative transfer in planetary atmospheres, the formation of molecular dimers is also believed to be the critical step for the onset production of larger clusters (Vehkamäki & Riipinen 2012) whose detailed growth processes are still relatively unknown. This was recently demonstrated in a kinetic study of water cluster formation at low temperature (Bourgalais et al. 2016). Such quantitative information is important for investigating condensation processes in cold planetary atmospheres through nucleation of molecular building blocks. Various theoretical methods were developed to estimate nucleation rates in order to characterize molecular growth. They are

⋆ E-mail: ludovic.biennier@univ-rennes1.fr

usually based either on thermodynamic (Diemand et al. 2013) or molecular (Schenter et al. 1999) approaches.

At the molecular level, nucleation is considered as a multistep process resulting from successive monomer addition reactions. Absolute nucleation rate predictions require rates for each elementary reaction step. However, detailed investigations of these elementary steps are scarce, essentially because such experimental measurements are challenging. A few works were devoted to a quantitative estimation of the formation kinetics of dimers, including benzene C_6H_6 (Hamon et al. 2000) using laser-induced fluorescence, anthracene $C_{14}H_{10}$ (Biennier et al. 2011) and pyrene $C_{16}H_{10}$ (Sabbah et al. 2010) using photoionization at 157 nm coupled to mass spectrometry, and, more recently, water vapor (Bourgalais et al. 2016) using electron impact ionization coupled to mass spectrometry. All these experiments employed the so-called CRESU (French acronym standing for Kinetics of Reactions in Supersonic Uniform Flows) technique to generate continuous cold uniform supersonic flows through de Laval nozzles.
Another approach for investigating cluster formation at low temperatures was adopted by Signorell and coworkers, using pulsed cold supersonic flows generated by de Laval nozzles, in which time evolution of propane (Ferreiro et al. 2016), toluene (Chakrabarty et al. 2017) and water (Lippe et al. 2018) cluster distributions were monitored at temperatures ranging from 42 to 56 K for propane, 48 to 77 K for toluene, and at 47 and 87 K for water. In these studies, the evolution of cluster sizes was derived from mass spectrometry ion signals following single photon ionization at 118 nm (13.8 eV). Such detailed observations are valuable to understand the mechanisms involved in the growth of clusters. They notably allow the critical cluster size range for nucleation to be determined. Yet they require molecular-level simulations for more detailed and quantitative information to be extracted on the growth mechanisms, and do not provide any quantitative information on the rate coefficients of formation of dimers or larger clusters.

The formation of dimers and their subsequent growth into larger clusters is of particular interest for Titan's atmosphere, where a rich organic inventory, as well as thick organic hazes are observed (Vuitton et al. 2019; West et al. 2014). Organic dimers may form in this atmosphere, however, no study thus far has attempted to evaluate the abundance and potential impact of such components. Cassini IR observations do reveal features that have not been interpreted by regular gas molecules but are considered to be an unknown condensate (Anderson & Samuelson 2011; Jennings et al. 2015), and their potential interpretation through dimer formation needs to be evaluated. Moreover, as temperature decreases rapidly in Titan's lower atmosphere, most of the formed photochemical products condense below ∼150 km, suggesting that larger clusters should readily form. However, this homogeneous nucleation mechanism would have to compete with the typically faster heterogeneous nucleation on the surface of the haze particles (Lavvas et al. 2011), and it is important to evaluate if cluster formation can provide a significant additional component to the haze population. Although the details of haze formation are unknown, it is well-established that ion-neutral chemical reactions in Titan's upper atmosphere allow for the rapid formation of macromolecules that subsequently nucleate, thus initiating the haze formation (Waite et al. 2007; Lavvas et al. 2013). If cluster formation can proceed fast enough to compete with the heterogeneous nucleation on the surface of the falling haze particles, then an additional formation mechanism has to be considered in the microphysics models of Titan's haze (Lavvas et al. 2010; Rannou et al. 2010).

In this study we experimentally investigate the formation kinetics of propane dimers at 23, 36 and 49 K, and use the derived rate coefficients to calculate the association and evaporation rates in order to estimate the abundance of propane dimers in Titan's lower atmosphere. Propane, originating from the methane photochemistry (Vuitton et al. 2019) is of special interest as it is at the crossroad of mass and abundance: smaller mass photochemical products (*e.g.* ethane) are more abundant but their binding energy would be too weak to support the formation of dimers at the conditions under investigation, while larger mass photochemical products (*e.g.* C_4H_{10}) are less abundant. Nitrile species are also produced in Titan's atmosphere (*e.g.* HCN, HC_3N, etc) and could more efficiently form dimers due to their polar nature. This could be the subject of future studies.

The experimental methods are described in Section 2. In Section 3 the various processes through which the propane clusters go before being detected in their ionized form in the present experiments are investigated in order to give a representative picture of the neutral clusters distribution in the cold supersonic flows. Estimated dimerization rate coefficients are given and discussed in Section 4. Theoretical determination of association and dissociation rate coefficients and their comparison with experimental data are presented in Section 5. In Section 6, the results are implemented in a photochemical model to perform a detailed evaluation of the dimer abundance in the low (< 200 km) atmosphere of Titan. Our conclusions are finally given in Section 7.

2 EXPERIMENTAL METHODS

Laboratory experiments were carried out using a CRESU machine developed in Rennes (Dupeyrat et al. 1985). The CRESU method has been previously employed to investigate the kinetics of homogeneous nucleation of condensable species (Hamon et al. 2000; Sabbah et al. 2010; Bourgalais et al. 2016) and only a brief overview with some details specific to this study are outlined here. A comprehensive description of the current setup is provided in the Supporting Information of Bourgalais et al. (2016).
In this work, we have explored the formation of propane clusters in cold and dense uniform supersonic helium flows, in which a small (< 1% of total flow density) and controllable amount of propane was introduced. Three different Laval nozzles with temperature, density and pressure characteristics given in Table 1, were employed to cover the 23–49 K temperature range.
The time evolution of the propane cluster densities in the flow was monitored by coupling the CRESU reactor with a time-of-flight mass spectrometer combined with an electron gun to ionize the clusters in an intermediate low-pressure chamber. Electron impact ionization and the detection of the propane clusters are discussed below.

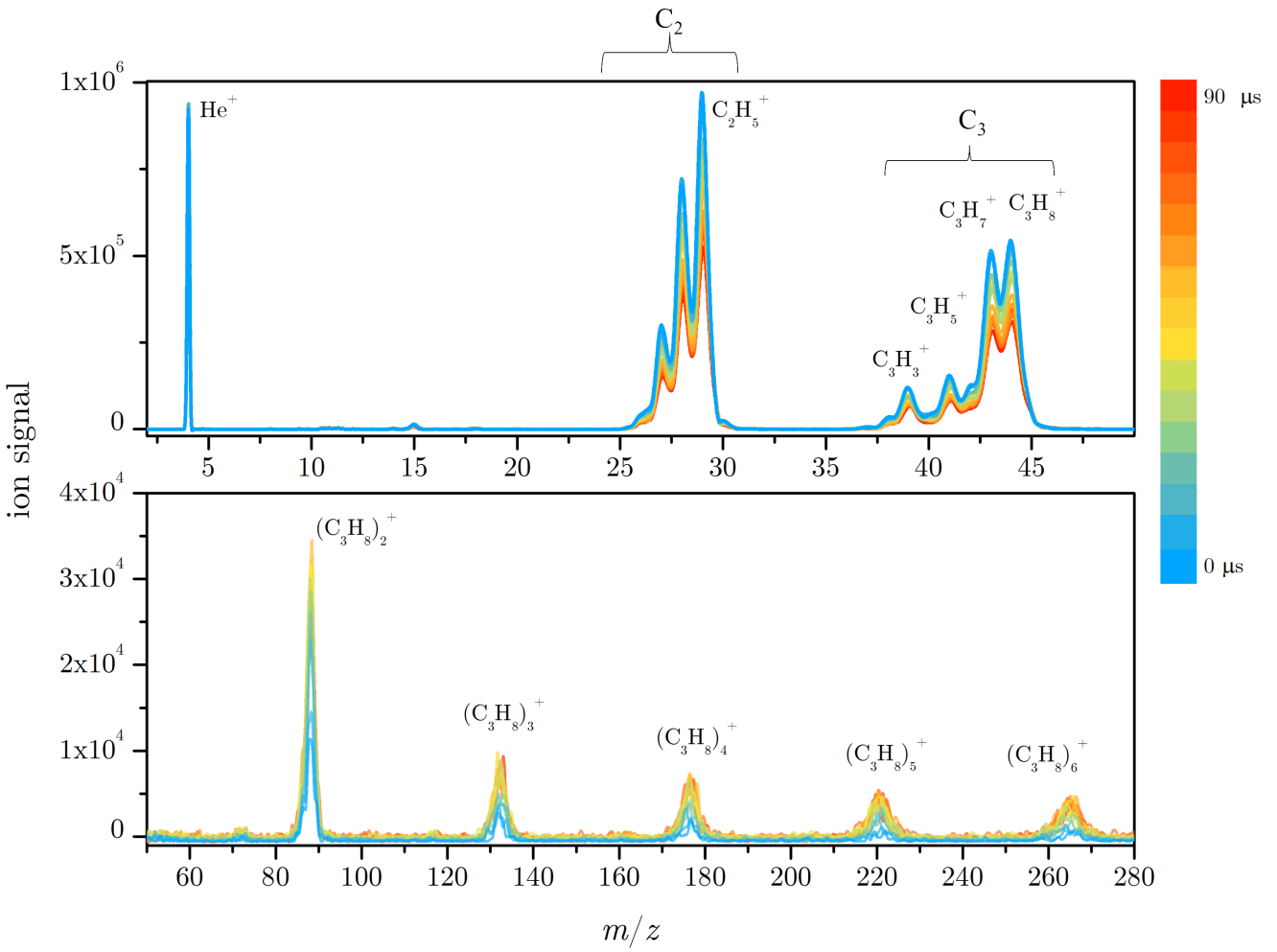

Figure 1. Time-of-flight mass spectra of helium uniform flow at 23 K seeded with propane with an initial density of 3.22×10^{14} cm^{-3} and for different reaction times in the 0–90 μs window.

T/K	[He]/10^{16} cm^{-3}	p/mbar	t_{max}/μs
22.9	4.75	0.18	103
36.1	5.26	0.29	140
49.1	10.45	0.78	92

Table 1. Experimental conditions for the three supersonic uniform flows used in this work; t_{max} corresponds to the flow hydrodynamic time. The errors on the temperature, the total flow density and the pressure chamber are under 5% at the level of the two standard deviations from the mean and are calculated from separate measurements of the impact pressure using a Pitot tube as a function of distance from the Laval nozzle.

3 IONIZATION AND DETECTION OF PROPANE CLUSTERS

3.1 Sampling, ionization and mass-selective detection

After a controllable reaction time, the cold and thermalized uniform flow is sampled to generate a molecular beam in which reactions are essentially stopped since the mean duration between successive collisions soars up to the microsecond scale. Propane clusters formed in the molecular beam are submitted to a transverse flux of 70 eV electrons, leading to a fraction of them being ionized. Immediately after ionization, the charged species are guided into the extraction zone after a short travel time that depends on their mass ($\sim (m/\text{amu})^{1/2}$ microseconds). From there the clusters are injected into the flight tube where they fly for tens of microseconds before impacting a multichannel plates detector. Impacting ions lead to a signal that is related to the ion population. The cluster content of the flow is inferred from the analysis of the mass spectra, which provide an image of the cluster population albeit with some distortion. Cluster ions are visible on mass spectra of He flows seeded with propane, as displayed for instance in Fig. 1 for the low temperature of 23 K. At short flight times, *i.e.* below 15 μs, the mass spectra show two groups of peaks assigned to C_2 and C_3 hydrocarbons. This mass pattern originates from sequential decay reactions of ionized propane (*e.g.* $C_3H_8^+ \longrightarrow C_3H_7^+$, etc.). At longer flight times, the mass spectra reveal a series of peaks that are assigned to stoichiometric propane clusters, *i.e.* of the $(C_3H_8)_n$ type. In order to reconstruct a faithful image of the neutral clusters distribution, it is necessary to identify and quantify the respective importance of the various possible processes that they go through before being detected in ionized form.

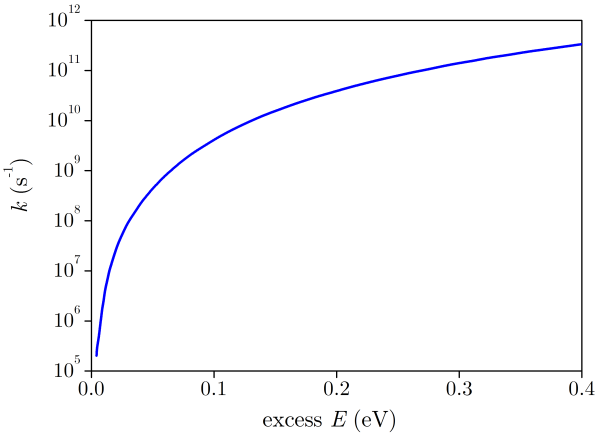

Figure 2. Calculated absolute evaporation rate (i.e. loss of a monomer) vs. excess energy for the cationic propane dimer $(C_3H_8)_2^+$.

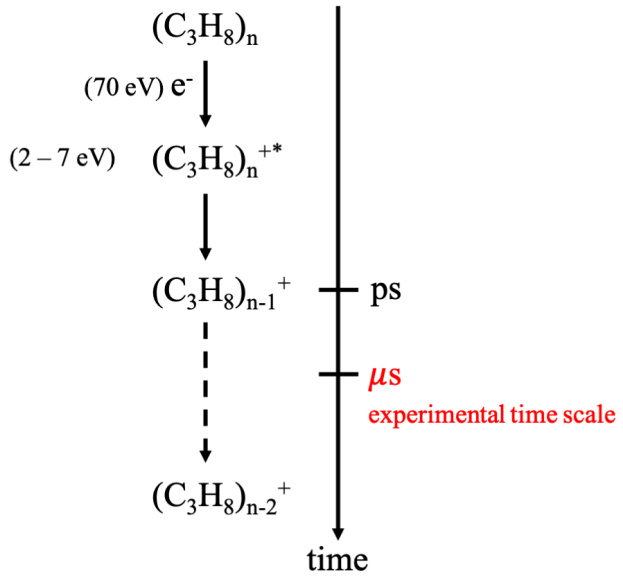

Figure 3. Dissociation dynamics of propane clusters $(C_3H_8)_n$ following electron impact ionization.

3.2 Dynamical aspects and fragmentation pattern

Various aspects of the fragmentation dynamics of ionized molecular clusters have been explored in the past, in particular for propane (Foltin et al. 1992), but many pieces of the puzzle are still missing. We provide below some elements on the the energetics and the dynamics of the processes involved.

3.2.1 Energy deposition in the dimer following ionization

For a neutral propane cluster, the sequence starts with electron impact ionization:

$$(C_3H_8)_n + e^- \longrightarrow (C_3H_8)_n{}^{+*} + e^- + e^- \quad (1)$$

Ionization itself occurs extremely fast upon electron impact as the time needed for an electron of 70 eV to travel 1 Å through a molecule is only about 2 $\times 10^{-17}$ s. The molecule being hit by the electron can be considered to be at rest because its thermal velocity of a few hundreds of $m{\cdot}s^{-1}$ is negligible compared to the speed of the electron rushing through (Gross 2006). In terms of energetics, firstly only a fraction of the energy of the impinging electron will contribute to ionize and heat the cluster as most of it is carried away with the electron itself after the collision. Secondly, the ionization process will take away the amount of energy corresponding to the adiabatic ionization potential of the dimer, which is 10.7 eV (See Sec. 3.2.2). Then, the minimum amount of excess energy remaining in the cationic dimer following ionization of the neutral dimer can be evaluated by performing electronic structure calculations. A realistic geometry for the neutral dimer was first obtained from classical simulations using the Amber ff94 force field. Density-functional theory calculations were then carried out using the double hybrid functional M06-2X and the aug-cc-pVDZ basis set for the cation in the doublet state, followed by a local optimization. The absolute vertical and adiabatic energies thus obtained are -237.7450 and -237.7745 Hartree, or a difference exceeding 0.8 eV or 18 kcal/mol. Qualitatively, this sets a lower bound to the excess energy deposited in the cationic cluster.

Weak intermolecular energies and any moderate redistribution will facilitate the evaporation of individual monomers, possibly before statistical equilibrium is established (Abdoul-Carime et al. 2015). The observation of stoichiometric cationic propane clusters in the mass spectra thus suggests that monomer evaporation is an important decay channel after ionization, even if a fraction of the energy deposited is sufficient to induce intramolecular covalent bond breaking. The energy deposited in the clusters that do not undergo intramolecular dissociation can be roughly evaluated as not exceeding a few eV per molecule.
Those findings are in agreement with recent studies of Irikura (2017) which combined experimental breakdown data from photoelectron-photoion-coincidence measurements and the Binary-Encounter Bethe (BEB) theory. These authors found that for tetrahydrofuran C_4H_8O and methane CH_4 the energy deposited by energetic electrons (> 25 eV) was below 20 eV. Assuming a complete relaxation to the electronic ground state of the ion and taking into account the adiabatic ionization energy, a corresponding energy deposited under 5 eV as vibrational excitation was estimated.

3.2.2 Dissociation lifetime of the cationic dimer

The structure of the cationic monomer was presumed to be that obtained by relaxation from the neutral geometry. The structure of the dimer cation was obtained via random sampling over the relative orientations of the two monomers. Higher level energies were determined from single point CCSD(T)-F12/cc-pVTZ-F12 calculations (Knizia et al. 2009; Peterson et al. 2008) at the MP2/cc-pVTZ optimized geometries. The CCSD(T)-F12/cc-pVTZ-F12//MP2-cc-pVTZ calculated zero-point corrected binding energy for the cationic dimer is -11.30 kcal/mol. The corresponding adiabatic ionization energies for the monomer and dimer are

11.0 and 10.7 eV, respectively.
The microcanonical dissociation rate coefficient for the cationic dimer was predicted with RRKM theory. The long-range transition state flux was evaluated with VRC-TST (Klippenstein 1992) employing direct MP2/cc-pVDZ determinations of the interaction energies. The reaction coordinate was presumed to be the distance between the two centers-of-mass. Rigid-rotor harmonic-oscillator (RRHO) approximations were used in the evaluation of the state density, but with one torsional mode treated as a free rotor. Such RRHO assumptions may introduce modest errors in the predicted rate (*e.g.*, a factor of 3), but the predicted magnitude and energy dependence of the dissociation rate should be at least qualitatively correct.
The high internal energy of the cluster leads to the rapid evaporation of a monomer, which is the lowest energy dissociation channel. According to calculations performed for the dimer, displayed in Fig. 2, evaporation will proceed very fast, on the ps time scale, as the estimated internal energy (a few eV) is off the chart. We will assume here as a reasonable hypothesis that only one monomer is evaporated after ionisation under the accessible laboratory time frame (a few tens of microseconds). For clusters larger than the dimer ($n \geq 3$) this means that the $(C_3H_8^+)_{n-1}$ ion images the $(C_3H_8)_n$ neutral population (cf. Figure 3).

3.2.3 Fragmentation pathways of the cationic dimer

The key question is then to distinguish the monomer ion fragments ($C_2H_x^+$, $C_3H_y^+$) tracing the neutral monomer C_3H_8 from those tracing the dimer $(C_3H_8)_2$. As far as we are aware, no electron-impact ionization mass spectrum for the propane dimer $(C_3H_8)_2$ is available in the literature. Fortunately some clues can be gathered from the monomer studies. In the 70-eV electron impact ionisation mass spectrum of the propane monomer, the two-carbon group dominates over the three-carbon group, with the $C_2H_5^+$ ion being the most abundant fragment (Linstrom & Mallard 2005). As was discussed at length above, the fragmentation pattern is tightly linked to the internal energy of the ion, and therefore to the impacting electron energy. The energy left in the remaining ionized monomer after evaporation of one unit from the dimer (secondary product) is lower than the energy deposited in the monomer directly, at least by an amount corresponding to the dissociation energy (a few kcal/mol). Consequently, the fragmentation pattern is likely to differ. In particular, the lower internal energy is expected to change the branching into the various exit channels (Chupka & Kaminsky 1961). In the study of Denifl et al. (2005) it was shown that it requires more energy to form $C_2H_5^+$ and $C_2H_4^+$ than $C_3H_7^+$ via electron impact ionization of neutral propane. Accordingly, the distribution of the fragments is expected to shift towards the C_3 group as the internal energy decreases (cf. Fig. 4).

The earlier investigation of Buck et al. (1988) on electron impact induced fragmentation of size selected ethylene clusters $(C_2H_4)_n$ at an electron energy of 100 eV hints towards such a behavior. In that work, the dimer $(C_2H_4)_2$ shows a fragmentation pattern in which the product size distribution is clearly shifted towards the higher masses of the C_2 group with *e.g.* the absence of C_2H. In our experiments, the

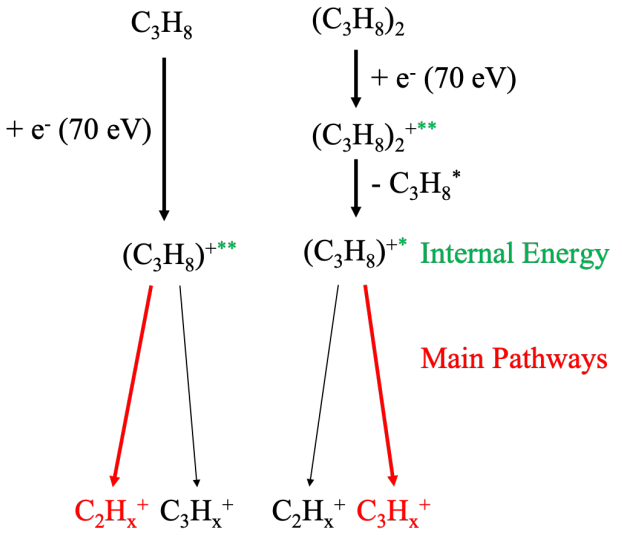

Figure 4. Fragmentation pathways for a propane molecule and a propane dimer ionized by an energetic electron

$C_3/(C_2+C_3)$ ratio derived from the mass spectra for different initial propane concentrations is not constant (Fig. 5) but appears to scale with propane concentration and is affected by the presence of cluster ions. Propane dimers are likely to be the main source of the excess of C_3 hydrocarbon ions. In the work of Buck et al. (1988) on ethylene clusters, the trimer and tetramer also produced some C_2 ions, however this channel amounts to a branching ratio of at most 46%, which contrasts with a value of 89% for the dimer.
Here, the first stages of nucleation are probed on the microsecond time scale and at low initial propane fractions. As a result, the size distribution is tilted towards low masses. By considering that in our case too, the fragmentation after evaporation will be limited to successive H loss channel (leading to C_3 hydrocarbons) with marginal C loss channel (decomposing into C_2 hydrocarbons), the dimer fraction defined by:

$$\zeta = \frac{[(C_3H_8)_2]}{[C_3H_8]} \tag{2}$$

can then be in principle expressed as:

$$\zeta(t) \simeq \left[\frac{C_3}{C_3+C_2}(t)\right]_{n_{\min}\to 0}^{n} \cdot \frac{\sigma_i^{C_3H_8}}{\sigma_i^{(C_3H_8)_2}} \tag{3}$$

where n is the propane concentration, C_2 and C_3 represent the ion signals into the respective channels, σ_i the ionisation cross sections, and

$$\left[\frac{C_3}{C_3+C_2}\right]_{n_{\min}\to 0}^{n} \tag{4}$$

the difference between the ratio at a given propane concentration n and at the lowest measured concentration $n_{\min}$ for which a signal can still be extracted, but in which aggregation is absent. Following the work of Deutsch et al. (2000) on small size clusters, we adopt an additivity rule in which the

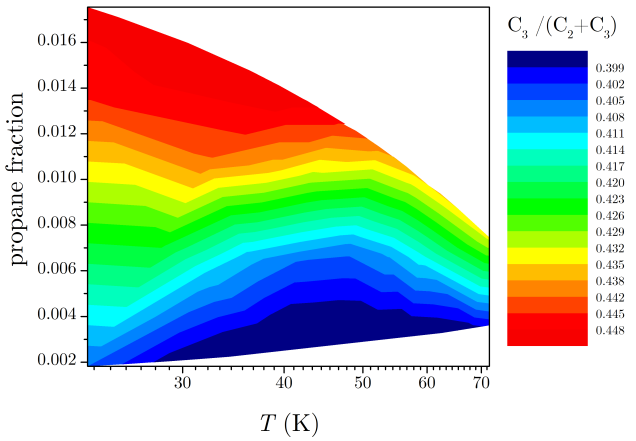

Figure 5. Evolution of the fragmentation pattern as indirect evidence of the presence of dimers. The experimental $C_3/(C_2+C_3)$ ratio shows some dependence on the flow temperature and initial propane fraction for reaction times above 40 μs. The dimer fraction ζ can be derived from the $C_3/(C_2+C_3)$ ratio assuming that the change in this ratio is mainly assigned to dimer fragments.

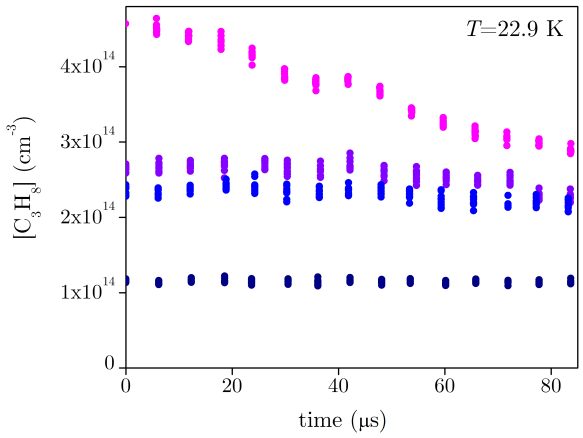

Figure 6. Propane monomer density vs time in a 22.9 K flow derived from time-of-flight mass spectrometry measurements. The He flow density is 4.75×10^{16} cm^{-3}. For initial propane fractions exceeding 0.5%, the monomer signal decays with time as monomers are consumed at the benefit of clusters.

electron impact ionization cross section of the neutral cluster of size m is about m times that of the neutral monomer:

$$\sigma_i^{(C_3H_8)_m} = m \cdot \sigma_i^{C_3H_8} \tag{5}$$

Unfortunately, the extraction of the dimer fraction rests on a non-background-free approach. As a consequence the associated noise gets very high and, in practice and despite our efforts, it should be considered as a qualitative tracer.

4 DIMER FORMATION RATE COEFFICIENT

The first step of these experiments was to determine the onset of propane nucleation. For this purpose, the time profile of the propane monomer concentration $[C_3H_8](t)$ was plotted at each flow temperature employed and for different initial densities (see Fig. 6 for an example at 23 K). At low initial propane monomer concentrations $[C_3H_8](t=0)$, no cluster ion peaks are seen and $[C_3H_8](t)$ is constant along the reaction time, indicating the absence of nucleation. When the initial concentration $[C_3H_8](t=0)$ increases, the propane monomer time profile $[C_3H_8](t)$ decays with time with a rate that scales with the initial concentration. This loss of monomer is due to the onset of propane nucleation. Cluster formation is initiated by dimerization, which is considered as a critical step conditioning the growth of clusters (Bourgalais et al. 2016; Vehkamäki & Riipinen 2012). Once formed, dimers go on to react rapidly with others monomers to form trimers and larger oligomers, as evidenced by mass spectra shown in Fig. 1. The onset of propane nucleation was obtained over the narrow range of 23–49 K under our experimental conditions, but not above, due to the limited initial reactant concentration (below 1%) allowed to maintain the uniformity of CRESU flows. Our measurements are also constrained by the short flow hydrodynamic time (100–200 μs).

The propane dimer grows from monomers, stabilized notably through collisions with He atoms to evacuate the energy acquired during the formation of the pair. The whole process can be summarised as:

$$C_3H_8 + C_3H_8 \xrightarrow{k_{1,1}} (C_3H_8)_2 \tag{6}$$

which can be generalized for larger clusters to:

$$(C_3H_8)_i + (C_3H_8)_{n+1-i} \xrightarrow{k_{i,n+1-i}} (C_3H_8)_{n+1} \tag{7}$$

From the listed reactions and considering the growth to be irreversible, we can write down the equations which govern the time evolution of the various species. In the most general way for the n^{th} cluster:

$$\begin{aligned} \frac{\mathrm{d}[(C_3H_8)_n]}{\mathrm{d}t} &= \sum_{i\leq\frac{n}{2}} k_{i,n-i}[(C_3H_8)_i][(C_3H_8)_{n-i}] \\ &- \sum_{i\geq1} (\delta_{n,i}+1)\, k_{n,i}[(C_3H_8)_n][(C_3H_8)_i] \end{aligned} \tag{8}$$

where $\delta_{n,i}$ is the Kronecker symbol. Basically, the first term is a production term, coming from smaller molecules while the second term is a consumption term forming larger clusters. For instance, the differential equation governing the evolution of the monomer is written:

$$\frac{\mathrm{d}[C_3H_8]}{\mathrm{d}t} = -\sum_{i\geq1} (\delta_{1,i}+1)\, k_{1,i}[C_3H_8][(C_3H_8)_i] \tag{9}$$

which gathers only loss terms. We go on with a similar equation for the dimer:

$$\begin{aligned} \frac{\mathrm{d}[(C_3H_8)_2]}{\mathrm{d}t} &= +k_{1,1}[C_3H_8]^2 \\ &- \sum_{i\geq1} (\delta_{2,i}+1)\, k_{2,i}[(C_3H_8)_2][(C_3H_8)_i] \end{aligned} \tag{10}$$

T (K)	$k_{1,1}$ (10^{-13} cm^3 s^{-1})	$[C_3H_8]_0$ (10^{14} cm^{-3})	[He] (10^{16} cm^{-3})	ζ
22.9	2 - 10	1.73 - 2.63	4.75	0.09
36.1	0.7 - 3.5	2.17	5.26	0.008
49.1	0.2 - 1	6.55	10.45	0.002

Table 2. Experimental rate coefficients for the dimerization of propane monomer at temperatures between 23 and 49 K derived from a kinetic model. ζ denotes the maximum calculated dimer fraction.

and for the trimer:

$$\frac{\mathrm{d}[(C_3H_8)_3]}{\mathrm{d}t} = +k_{1,2}[C_3H_8][(C_3H_8)_2] - \sum_{i\geq 1} k_{3,i}[(C_3H_8)_3][(C_3H_8)_i] \quad (11)$$

From there, we build a simple kinetic model with the above equations to reproduce the time evolution of the clusters up to the tetramer. The ultimate objective is to derive the $k_{1,1}$ reaction rate, which can be considered at low temperature as the nucleation bottleneck, i.e. the rate governing the kinetics of the whole process since it is the slowest. The procedure consists in numerically solving a set of four coupled differential equations. The dimer time evolution is considered only qualitatively as the non-background-free method employed to extract the data (see Sec. 3.2.3) leads to strong uncertainties. In spite of this missing piece of information, the output data remain consistent and robust.

Ingredients in the model are kept simple. The rates $k_{i,j}$ for forming clusters larger than $i + j \geq 4$ are allowed to only vary in a 3–5×10^{-10} cm^3 s^{-1} window for all flow temperatures considered. In addition, the inequality $k_{1,1} < k_{1,2} < k_{1,3}$ is enforced since adding a monomer to a dimer (trimer) is more efficient than adding a monomer to a monomer (dimer).

The calculated time-evolutions obtained with the model are displayed in Fig. 7 for an He flow at 22.9 K and for an initial monomer concentration $[C_3H_8](t = 0) = 2.63\times10^{14}$ cm^{-3} as an illustration. The set of results for the dimerization rate coefficient $k_{1,1}$ are gathered in Table 2. The derived rates exhibit large uncertainties with typically a factor of 5 between the lowest and the highest values. They nevertheless provide reasonable orders or magnitude.

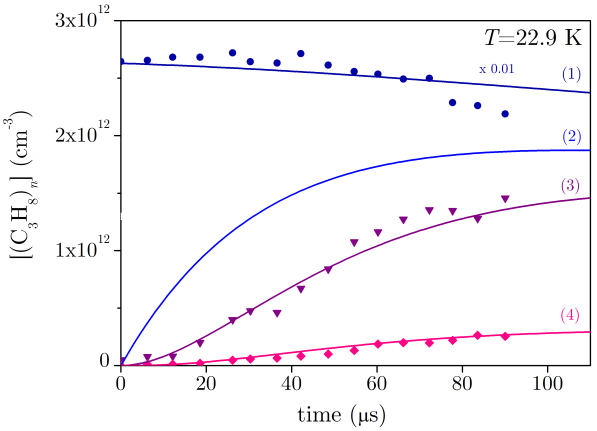

Figure 7. Calculated and experimentally measured time evolution of propane monomer and small clusters up to tetramer ($n = 4$). Flow conditions: $T = 22.9$ K and [He]=4.75 ×10^{16} cm^{-3}. Intial propane monomer density: 2.63×10^{14} cm^{-3}. The calculated and measured monomer signals ($n = 1$) have been scaled for illustrative purpose by a factor of 0.01. Only the calculated profile is displayed for the dimer ($n = 2$) as the time evolution derived from experiments remains qualitative (see Sec. 3.2.3).

5 THEORETICAL EVALUATION OF ASSOCIATION AND DISSOCIATION RATES

The rovibrational properties of the reactants and the complexes were determined at the MP2/cc-pVTZ level. For the dimer complex, the optimized structure was again obtained by further optimizing the lowest energy geometry obtained in a random sampling over interfragment orientations. Higher level energies were determined from single point CCSD(T)-F12/cc-pVTZ-F12 calculations at the MP2/cc-pVTZ optimized geometries. The zero-point corrected dimer binding energy is predicted to be -1.33 kcal/mol.

Thermal kinetic predictions were obtained from a master equation treatment implementing VRC-TST fluxes for the transition states, simple rigid rotor harmonic oscillator estimates for the partition functions and state densities of the complexes, Lennard-Jones collision cross sections, and exponential down energy transfer probabilities. The long-range transition state flux was evaluated with VRC-TST (Klippenstein 1992) employing direct MP2/cc-pVTZ determinations of the interaction energies. The reaction coordinate was presumed to be the distance between the two centers-of-mass. The lack of prior studies of the effective size for a van der Waals dimer (here the Lennard Jones collision cross section is estimated from σ_{dimer}=10 Å, $\varepsilon_{\mathrm{dimer}}$=400 cm^{-1} and σ_{He}=2.55 Å , $\varepsilon_{\mathrm{He}}$=7 cm^{-1}), and of the temperature dependence of the average downwards energy transfer at low temperatures [here set as 200 $(T/298\ \mathrm{K})^{0.5}$ cm^{-1}], leads to considerable ambiguity in the final rate estimates. Finally, we employ a correction factor of 3.3 to account for anharmonicities on the vibrational density of states for the complex, with this last factor obtained from a fit to experimental data. While all these values are reasonable, their ambiguity leads to significant uncertainties in the final rate estimates (*e.g.*, perhaps a factor of 4 or more).

Despite the aforementioned limitations, as seen in Fig. 8, this master equation-based model is able to quantitatively reproduce the full set of experimental observations, which lends some credence to both the theoretical model and the experimental analysis.

6 PROPANE DIMER FORMATION IN TITAN'S LOWER ATMOSPHERE

In Titan's atmosphere, Cassini observations reveal that the highest propane density lies between 100 and 150 km, before the onset of condensation at lower altitudes (Vinatier et al. 2010). Therefore, we anticipate that the propane dimer density will be maximum near this range as well. The local atmospheric conditions (∼ 120–170 K, 1–10 mbar) at this altitude range are different from those for the retrieved as-

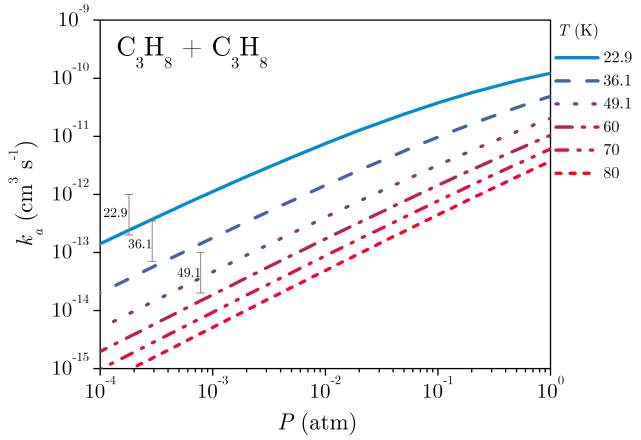

Figure 8. Calculated and experimental C_3H_8 + C_3H_8 association rates vs. temperature and pressure.

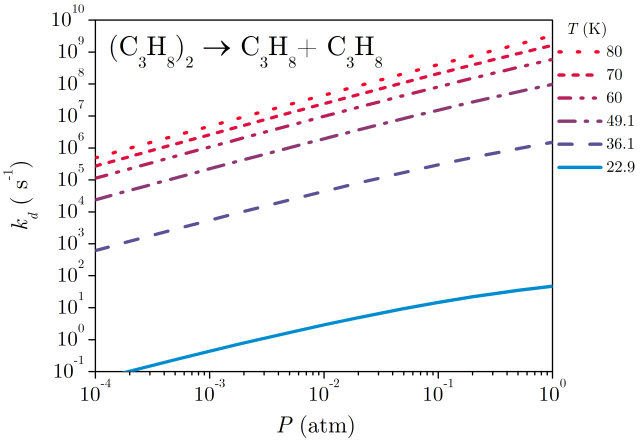

Figure 9. Calculated $(C_3H_8)_2 \rightarrow C_3H_8$ + C_3H_8 dissociation rates vs. temperature and pressure.

sociation and dissociation rates, thus an extrapolation in temperature is required. Moreover, in order to evaluate the dimer population with a photochemical model we need to transform the above derived rates into a temperature- and pressure-dependent form that will allow to represent the dimer formation and loss rates at all required conditions. For the association reaction we use the standard Troe formula (Troe 1979) where the reaction rate at temperature T and atmospheric density [M] is described as:

$$k(T,[\mathrm{M}]) = \frac{k_0[\mathrm{M}]}{1+k_0[\mathrm{M}]/k_\infty} F_c^{(1+\log(k_0[\mathrm{M}]/k_\infty)^2)^{-1}} \quad (12)$$

with

$$k_0[\mathrm{cm^6 s^{-1}}] = 10^{-25}\left(\frac{T}{\mathrm{K}}\right)^{-3.31} \exp(-14.5\ \mathrm{K}/T) \quad (13)$$

for the low pressure limit,

$$k_\infty[\mathrm{cm^3 s^{-1}}] = 1.9\times10^{-10}\left(\frac{T}{\mathrm{K}}\right)^{0.146} \exp(-2.1\ \mathrm{K}/T) \quad (14)$$

for the high pressure limit, and $F_c = 0.4$. For the dissociation rate we use the formula:

$$k_{diss} = k_\delta[\mathrm{M}] \quad (15)$$

with

$$k_\delta[\mathrm{cm^3 s^{-1}}] = 7839\left(\frac{T}{\mathrm{K}}\right)^{-5.27} \exp(-765.9\ \mathrm{K}/T) \quad (16)$$

to describe the dimer dissociation rate at different conditions.

We use these rates in a photochemical model to evaluate the abundance of propane dimers (Lavvas et al. 2008a,b). The model solves the continuity equation for the main hydrocarbon species, taking into account atmospheric mixing and molecular diffusion, as well as the condensation of the species once their individual saturation limits are reached. The model is updated with the latest chemical networks for Titan's atmosphere from Vuitton et al. (2019) where further information for the processes leading to the formation of C_3H_8 and other photochemical products in Titan's atmospheres can be found. Our simulated propane mixing ratio (Fig. 10) is consistent with the Cassini/CIRS observations in the lower atmosphere (Vinatier et al. 2010), which reveal a quasi-constant mixing ratio of $\sim10^{-6}$. Our simulated profile rapidly decreases below 100 km altitude as the local drop in Titan's atmospheric temperature leads to the rapid condensation of most photochemical products, including propane. In these calculations, condensational loss is treated in terms of the super-saturation of each species evaluated based on the saturation vapour pressure of each gas at the temperature of each altitude, i.e. the system relaxes to the saturation limit of each component (Lavvas et al. 2008a).

At these conditions, our calculations demonstrate that the corresponding $(C_3H_8)_2$ mixing ratio remains small at all altitudes and reaches a maximum mixing ratio of $\sim10^{-17}$ near 100 km (Fig. 10). At lower altitudes the condensation loss of propane monomers limits the abundance of dimers. This abundance, corresponding to a maximum density of $\sim$10 dimers cm^{-3}, is too small to be detected in the Cassini/CIRS data. Although the detection limit of each species can vary depending on its spectroscopic properties, a typical mixing ratio detection limit for the latter instrument is at the ppb (10^{-9}) range (Nixon et al. 2010). Therefore we can conclude that propane dimers will not have significant implication in the radiation transfer in Titan's atmosphere considering their predicted low abundance.

The population of dimers before the onset of condensation constrains the population of nuclei that will rapidly grow to larger clusters once super-saturation conditions are reached. Our simulated density of dimers is larger than the density of haze particles in Titan's lower atmosphere ($\sim$1cm^{-3} according to Tomasko et al. 2008; Doose et al. 2016). However, we need to consider that heterogeneous nucleation is faster than homogeneous nucleation. Classical nucleation theory (Pruppacher & Klett 1978) indicates that at the conditions under investigation heterogeneous nucleation is many orders of magnitude more efficient than homogeneous nucleation (Fig. 11). Our calculations suggest that irrespective of the particle size (in the range of 0.1–1 μm) and for various values of the contact angle between the propane condensate and the haze particle surface, heterogeneous nucleation starts at super-saturation values that

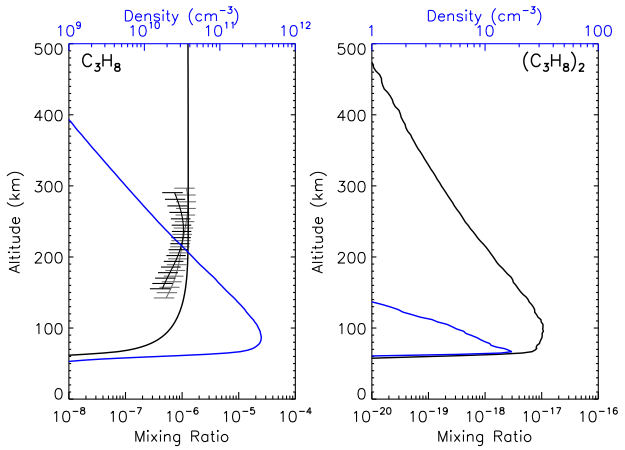

Figure 10. Simulated propane C_3H_8 and propane dimer $(C_3H_8)_2$ abundances in Titan's lower atmosphere. Black lines represent the mixing ratios and blue lines the corresponding number densities of each component. The gray and black curves with error bars correspond to the retrieved C_3H_8 stratospheric abundance from Cassini observations at mid latitudes (30N and 39N, respectively, from Vinatier et al. 2010), which are more representative of our disk-averaged simulations.

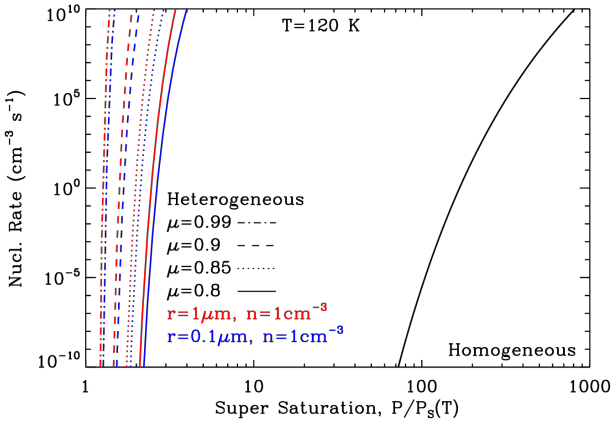

Figure 11. Predictions of classical nucleation theory for the homogeneous (black line) and heterogeneous (red and blue lines) nucleation rates of C_3H_8. Different colours present evaluations of heterogeneous nucleation rates at different radius spherical particles, while different broken lines reveal the dependence of the heterogeneous rate on the contact angle between the condensate and the substrate.

are more than 50 times lower than the super-saturation required for the onset of homogeneous nucleation (∼nucleation rate of 1 cm^{-3}s^{-1}). The simulations show that the higher abundance of dimers compared to haze particles will not compensate for the difference in the rates of the two mechanisms and that propane molecules will more efficiently condense on the surface of the falling haze particles than form new pure-condensate particles.

7 CONCLUDING REMARKS

Owing to a diversity of processes occuring simultaneously, the chemical and physical pathways leading to the formation and growth of particles in Titan's low atmosphere provide a wide open field of investigation. In this study we considered the propensity of propane to form homogeneous clusters through nucleation. Our work was motivated by the large abundance of neutral hydrocarbons in Titan's atmosphere and their high level of saturation. Propane, initially detected and identified in Titan's atmosphere after the Voyager 1 flyby (Hanel et al. 1981; Maguire et al. 1981) shows a constant uniform abundance at the ppm level throughout the stratosphere in recent analyses (Vinatier et al. 2015; Coustenis et al. 2018; Lombardo et al. 2019). The results of the photochemical model used in this study display a consistent maximum of 10^{-6} in the stratospheric mixing ratio above 100 km. Below this altitude, the abundance starts to decrease drastically due to the expected onset of propane condensation (Lavvas et al. 2011). The model output predicts a maximum propane dimer density near 100 km but below the ppb detection limit of the CIRS instrument. Moreover, the difference between the monomer and the dimer mixing ratios is quite significant (∼10 orders of magnitude around 60 km) and shows that condensates coming from homogeneous nucleation of the most abundant alkanes appear to be irrelevant for the formation of new particles, while the possible implications of dimer formation on the atmospheric properties seems negligible. However those investigations should be extended to other abundant species that carry dipoles, often N-bearing atoms, which could thus form stronger intermolecular bonds.

The current work has also exposed some limits of electron-impact ionization mass spectrometry for the study of quantitative cluster formation in the case of multiple overlapping ionization product channels. We were in particular unable to identify a reliable tracer of the dimer, but had to rely on a number of assumptions (evaporation pattern, ionization cross sections...), and the derived rates were tainted with large uncertainty. Future studies will be performed with a tunable photon energy source (provided *e.g.* by synchrotron radiation) for threshold ionisation to limit evaporation and fragmentation. Such an experiment combining uniform supersonic flows and time-of flight mass spectrometry with photoionization, dubbed CRESUSOL, has recently been designed and is now operational.

ACKNOWLEDGEMENTS

This work was supported by the CNRS-INSU Programme National de Planétologie (PNP). LB thanks Paul Scheier and Musahid Ahmed for helpful discussions regarding the ionized cluster fragmentation dynamics. The contribution from SJK is supported by the U.S. Department of Energy, Office of Science, Office of Basic Energy Sciences, Division of Chemical Sciences, Geosciences, and Biosciences under Contract No. DE-AC02-06CH11357 (BES Gas Phase Chemical Physics Core Program).

REFERENCES

Abdoul-Carime H., et al., 2015, Angewandte Chemie, International Edition, 54, 14685

Anderson C. M., Samuelson R. E., 2011, Icarus, 212, 762

Biennier L., Sabbah H., Chandrasekaran V., Klippenstein S. J., Sims I. R., Rowe B. R., 2011, Astronomy and Astrophysics, 532, 40

Bourgalais J., Roussel V., Capron M., Benidar A., Jasper A., Klippenstein S., Biennier L., Le Picard S. D., 2016, Physical Review Letters, 116, 113401

Buck U., Lauenstein C., Meyer H., Sroka R., 1988, Journal of Physical Chemistry, 92, 1916

Chakrabarty S., Ferreiro J. J., Lippe M., Signorell R., 2017, Journal of Physical Chemistry A, 121, 3991

Chupka W. A., Kaminsky M., 1961, Journal of Chemical Physics, 35, 1991

Coustenis A., Jennings D., Achterberg R., Bampasidis G., Nixon C., Lavvas P., Cottini V., Flasar F., 2018, Astrophysical Journal Letters, 854, L30

Daniel J. S., Solomon S., Kjaergaard H. G., Schofield D. P., 2004, Geophysical Research Letters, 31

Denifl S., et al., 2005, Chemical Physics Letters, 402, 80

Deutsch H., Becker K., Matt S., Märk T. D., 2000, International Journal of Mass Spectrometry, 197, 37

Diemand J., Angélil R., Tanaka K. K., Tanaka H., 2013, Journal of Chemical Physics, 139, 074309

Doose L. R., Karkoschka E., Tomasko M. G., Anderson C. M., 2016, Icarus, 270, 355

Dupeyrat G., Marquette J., Rowe B., 1985, Physics of Fluids (1958-1988), 28, 1273

Ferreiro J. J., Chakrabarty S., Schläppi B., Signorell R., 2016, Journal of Chemical Physics, 145, 211907

Foltin M., Grill V., Rauth T., Herman Z., Märk T., 1992, Physical Review Letters, 68, 2019

Frommhold L., Samuelson R., Birnbaum G., 1984, Astrophysical Journal, 283, L79

Gross J. H., 2006, Mass spectrometry: a textbook. Springer Science & Business Media

Hamon S., Le Picard S. D., Canosa A., Rowe B. R., Smith I. W., 2000, Journal of Chemical Physics, 112, 4506

Hanel R., et al., 1981, Science, 212, 192

Irikura K. K., 2017, Journal of Physical Chemistry A, 121, 7751

Jennings D. E., et al., 2015, The Astrophysical Journal Letters, 804, L34

Klippenstein S., 1992, Journal of Chemical Physics, 96, 367

Knizia G., Adler T. B., Werner H.-J., 2009, Journal of Chemical Physics, 130, 054104

Lavvas P., Coustenis A., Vardavas I., 2008a, Planetary and Space Science, 56, 27

Lavvas P., Coustenis A., Vardavas I., 2008b, Planetary and Space Science, 56, 67

Lavvas P., Yelle R. V., Griffith C. A., 2010, Icarus, 210, 832

Lavvas P., Griffith C., Yelle R., 2011, Icarus, 215, 732

Lavvas P., et al., 2013, Proceedings of the National Academy of Sciences, 110, 2729

Linstrom P. J., Mallard W. G., eds, 2005, NIST Chemistry WebBook, NIST Standard Reference Database Number 69. National Institute of Standards and Technology, Gaithersburg MD, 20899, http://webbook.nist.gov

Lippe M., Chakrabarty S., Ferreiro J. J., Tanaka K. K., Signorell R., 2018, Journal of Chemical Physics, 149, 244303

Lombardo N. A., Nixon C. A., Achterberg R. K., Jolly A., Sung K., Irwin P. G., Flasar F. M., 2019, Icarus, 317, 454

Maguire W., Hanel R., Jennings D., Kunde V., Samuelson R., 1981, Nature, 292, 683

Nixon C. A., et al., 2010, Faraday Discussions, 147, 65

Peterson K. A., Adler T. B., Werner H.-J., 2008, Journal of Chemical Physics, 128, 084102

Pruppacher H. R., Klett J. D., 1978, Microphysics of Clouds and Precipitation. Reidel Publishing Group

Rannou P., Cours T., Le Mouélic S., Rodriguez S., Sotin C., Drossart P., Brown R., 2010, Icarus, 208, 850

Sabbah H., Biennier L., Klippenstein S. J., Sims I. R., Rowe B. R., 2010, Journal of Physical Chemistry Letters, 1, 2962

Schenter G. K., Kathmann S. M., Garrett B. C., 1999, Physical Review Letters, 82, 3484

Tomasko M. G., Doose L., Engel S., Dafoe L. E., West R., Lemmon M., Karkoschka E., See C., 2008, Planetary And Space Science, 56, 669

Troe J., 1979, The Journal of Physical Chemistry, 83, 114

Vaida V., Kjaergaard H. G., Feierabend K. J., 2003, International Reviews in Physical Chemistry, 22, 203

Vehkamäki H., Riipinen I., 2012, Chemical Society Reviews, 41, 5160

Vigasin A., Mokhov I., 2017, Izvestiya, Atmospheric and Oceanic Physics, 53, 164

Vinatier S., et al., 2010, Icarus, 205, 559

Vinatier S., et al., 2015, Icarus, 250, 95

Vuitton V., Yelle R. V., Klippenstein S. J., Hörst S. M., Lavvas P., 2019, Icarus, pp 1–75

Waite J. H., Young D. T., Cravens T. E., Coates A. J., Crary F. J., Magee B., Westlake J., 2007, Science, 316, 870

West R., Lavvas P., Anderson C., Imanaka H., 2014, Titan Haze. Cambridge University Press Cambridge, UK

This paper has been typeset from a TEX/LATEX file prepared by the author.